J. Phys. D: Appl. Phys. 26 (1993) 222–230. Printed in the UK

Picosecond resolved evolution of laser breakdown in gases

Lloyd M Davis, Li-Qiang Li and Dennis R Keefer

Center for Laser Applications, University of Tennessee Space Institute, Tullahoma, TN 37388, USA

Received 26 February 1992, in final form 8 September 1992

Abstract. Subpicosecond pulses from a synchronously pumped dye laser were used to collinearly probe the absorption of laser breakdown plasmas formed by focusing longer (60 ps) 532 nm pulses from a regenerative amplifier into a cell containing helium, argon or nitrogen. The absolute time delay between the 532 nm pulses and the probe pulses was varied in order to measure the initiation time and the rate of growth of the plasma for different pressures and breakdown pulse energies. In general, at the higher pressures, for which cascade ionization processes are expected to dominate, the onset of the plasma is found to be quite abrupt compared with the duration of the breakdown pulse. The initiation time is earlier and the rate of growth is faster if the breakdown pulse energy or pressure is increased. For argon and nitrogen at lower pressures, slow growth of the plasma can continue for hundreds of picoseconds after the breakdown pulse has passed, indicating that relaxation from a non-equilibrium state occurs.

1. Introduction

Breakdown at the focus of a pulsed laser beam has been observed since the advent of the ruby laser nearly 30 years ago, and a considerable body of literature aimed at understanding the physical mechanisms for optical breakdown in transparent media has since been written [1, 2]. Breakdown in gases can be caused by direct ionization or, when the pressure is sufficiently high, by cascade or avalanche growth of ionization due to inverse Bremsstrahlung absorption of energy by free electrons followed by collisional ionization [3–5]. Direct ionization is generally due to multiphoton absorption [6, 7] but at longer laser wavelengths, where a larger number of photons would be needed, or at large laser intensities, it may be due to the tunnelling of the electrons in the presence of the strong laser field [8–11]. Photoionization of excited intermediate atomic or molecular states and molecular dissociation are also important for certain gases [3, 12–14].

To date, experiments have centred largely on the measurement of the breakdown threshold for various conditions [15–19]. 'Breakdown' is usually defined by the optical detection of the luminous plasma emission or the acoustical detection of the shock wave.

For longer, i.e. nanosecond, laser pulse lengths, the threshold is generally found to be inversely dependent on the pulse length and on the pressure, indicating that a collisional mechanism for the onset of breakdown is predominant. For shorter laser pulses ($\leqslant 10$ ps) or low pressures, the breakdown threshold is considerably higher and only weakly dependent on pressure, indicating that direct ionization by the laser pulse is the predominant mechanism.

It is well recognized that the various mechanisms may act simultaneously and that their relative contributions not only depend on the initial conditions but also change during the growth of the plasma. Indeed, theoretical modelling of the laser-induced breakdown has developed to quite a sophisticated level [19–21] and may include all these effects and predict the growth of the plasma with time. However, the point of comparing theory with experiment is generally the dependence of the breakdown threshold on the initial conditions of pressure, laser wavelength and intensity and type of gas.

In some experiments, the temporal evolution of the breakdown process has been followed with nanosecond resolution [22, 23] and Schlieren images of a laser plasma ~ 20 ps [24] and many nanoseconds [25] after breakdown have been published. Laser breakdown plasmas have been used to produce ultrafast shutters [26–29].

In this article, we give the results of pump and probe experiments which permit the growth of a plasma in a gas to be followed with a time resolution of a few picoseconds. In addition, we have monitored the relaxation time of the plasma by measuring the absorption of probe pulses which pass many nanoseconds after the plasma is formed.

0022-3727/93/020222+09$07.50

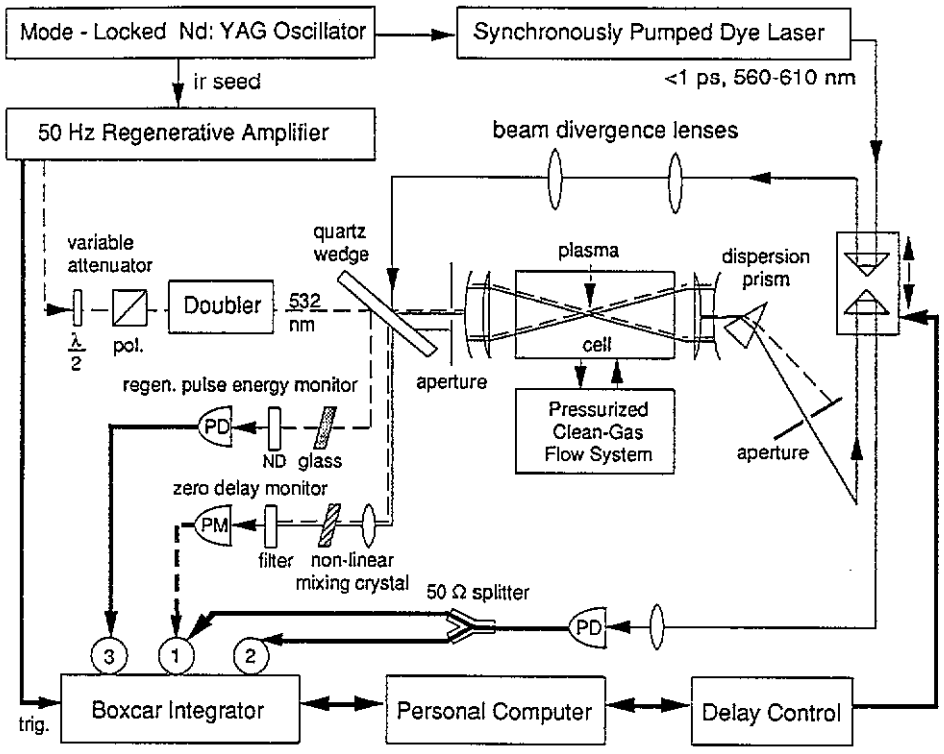

Figure 1. Pump and probe experiment to measure the initiation of laser-induced plasmas. ($\lambda/2$: half-wave plate, pol.: Glan–Taylor polarizer, PD: photodiode, PM: photomultiplier, ND: neutral density filter.)

2. Experimental apparatus

The experimental set-up, as shown in figure 1, consists of a standard collinear 'pump and probe' configuration. The laser-breakdown plasma is formed by the 532 nm pulses from a Nd:YAG regenerative amplifier (Continuum RGA-60-50) while the subpicosecond pulses, from a synchronously pumped hybrid-modelocked dye laser (Coherent 702-1), are used to probe the absorption of the plasma versus temporal delay.

The dye laser produces pulses tunable from 565 nm to 605 nm at a repetition rate of 76 MHz, each with a pulse energy of about 2 nJ and with an autocorrelation width of 1.0 ps. The regenerative amplifier produces pulses at a repetition rate of 50 Hz with a pulse energy of about 40 mJ at 1064 nm and with a width of about 90 ps. These pulses pass through a variable attenuator consisting of a rotatable half-wave plate and a dielectric polarizer before being frequency doubled in a KDP crystal to yield 532 nm pulses with energies of up to 12 mJ. Because both the regenerative amplifier and the synchronously pumped dye laser are pumped by the same acousto-optically mode-locked Nd:YAG oscillator (Coherent Antares 76-s), the pulse trains have a well defined timing with respect to each other, even though they have considerably different repetition rates.

The 532 nm beam from the regenerative amplifier is collinearly combined with the dye laser beam using an uncoated quartz substrate. Both beams are vertically polarized and the substrate acts as a 10% : 90% beam splitter at 45°. The portion of 532 nm beam which is split from the first surface passes through a neutral density filter to a photodiode (HP-4203), which is calibrated with respect to a pulse-energy probe (Lasermetrics RJ-7200/RJP-734) placed immediately after the first window of the sample cell. The pulse-to-pulse energy fluctuations are found to be 5–10%.

Approximately 80% of the 532 nm pulse intensity and 10% of the dye laser pulse intensity reflected from the second surface of the quartz substrate are passed through the aperture to the sample cell. The beams are focused by a plano-convex lens with focal length of 7.84 cm. The diameter of the beams at the lens is approximately 0.46 cm resulting in an effective f number of $f/17$. A razor edge is transversely translated across the focal plane of the 532 nm beam and the transmitted pulse energy is well fitted by a Gaussian error function, yielding a beam waist of $7.8 \pm 0.2\ \mu$m. The beam divergence of the dye laser beam at the focusing lens is adjusted by passing it through a pair of lenses so that it focuses at the same plane as the 532 nm beam and with about the same waist. Thus at the sample, the peak intensity of the probe pulses is approximately five orders of magnitude less than that of the breakdown pulses.

Following these initial set-up measurements, the sample cell is installed. The cell consists of an aluminium block with uncoated quartz windows at each end and a third window on the side for visual observation of the plasma. A digital pressure gauge (Omega

DPG-500) is used to measure pressures from 7 to 150 psi while a vacuum gauge (Edwards 8800) is used for lower pressures. The inlet port is attached through a cold trap and needle valve to a regulator and gas supply, and the outlet port is attached through another needle valve to either a liquid nitrogen trap and roughing pump or a molecular diffusion pump, which is used for completely purging the cell.

Research grade gases with < 30 ppm impurities were used. Our early experiments indicated that it is important to take considerable care to remove impurities from the cell and gas lines as these may influence the breakdown thresholds and the behaviour of the breakdown [30]. In addition, because the accumulation of metastable states can influence breakdown, in all experiments the gas was circulated away from the focal volume by letting gas in through one port and out through the other [22].

The transmitted laser beams are recollimated as they emerge from the cell and the dye laser probe pulses are separated by a dispersion prism and aperture and are eventually focused onto a fast photodiode (Antel AR-S2). If there is no plasma present, this photodiode simply sees a train of dye laser pulses at a repetition rate of 76 MHz. However, when the regenerative amplifier is turned on, every 20 ms a plasma is formed and the dye laser pulse which arrives at this time (the diagnostic pulse) is absorbed, as shown schematically in figure 2. Because fluctuations in the dye laser power occur on a time-scale no faster than tens of milliseconds, the pulse that arrives immediately prior to the formation of the plasma can be used as an accurate reference for the measurement of the transmission ratio of the plasma. Thus, as shown in figure 1, the signal from the fast photodiode is split at a 50 Ω power splitter and is directed to two separate channels of a boxcar integrator (Princeton Applied Research 4402 with 4422 integrators). The boxcar is triggered by the sync-output pulse from the regenerative amplifier and is used in static gate mode with 2 ns windows and time delays set to capture the amplitude of the diagnostic pulse in channel 1 and that of the reference pulse in channel 2. In addition, the amplitude of the photodiode pulse which monitors the pulse energy of the regenerative amplifier is recorded in channel 3.

The time delay of the dye laser pulses with respect to the regenerative amplifier pulse can be changed by an adjustable optical delay line, using a motorized translator (Burleigh 7000/IW-712). As shown in figure 1, a compensating delay is used so that pulses from the fast photodiode always arrive at the boxcar with the same time delay with respect to the trigger signal. The translator is programmed to take 2 ps (0.3 mm) steps and at each step the plasma transmission ratio from five breakdown pulses is averaged. The final result is obtained as the average of four bi-directional scans of the translator, with a 1 ps delay offset between the forward and backward scans.

In order to find the position of the translator for which there is zero absolute time delay between the

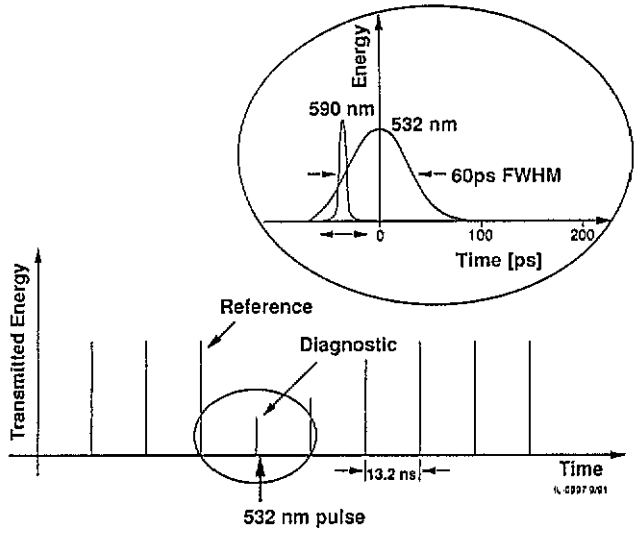

Figure 2. Timing relationship between the 532 nm breakdown pulse and the dye laser pulses.

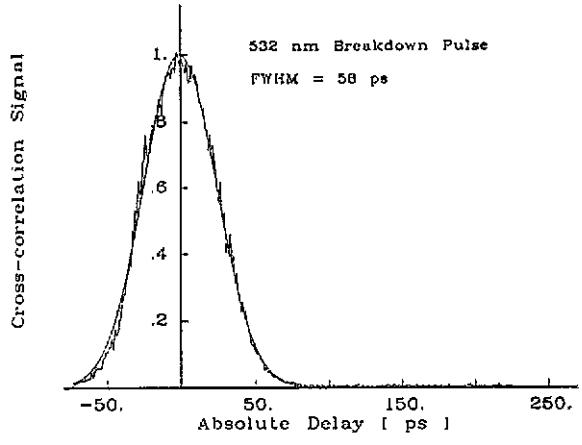

Figure 3. Cross correlation between the 532 nm breakdown pulses and the dye laser diagnostic pulses.

dye laser diagnostic pulse and the centre of the breakdown pulse (as shown in the inset in figure 2), the cross-correlation of the two beams is measured using a nonlinear crystal. The regenerative amplifier is considerably attenuated and 10% of the 532 nm beam together with 80% of the dye laser beam, obtained from the opposite output of the quartz substrate, are combined at a KDP (71° cut) crystal, which is angle-tuned so as to obtain the sum frequency. The same data acquisition and averaging scheme used to collect the pump and probe data is also used to obtain the cross-correlation function, except that the photomultiplier which measures the sum-frequency signal gives relatively slow microsecond output pulses so that a 1 μs gate width is used on the boxcar integrator. As the translator scans, the cross-correlation between the (< 1 ps) dye laser pulses and the 532 nm pulses is obtained, as shown in figure 3. A gaussian fit to this curve allows the position of the translator corresponding to zero delay to be determined. It also yields the pulse width of the 532 nm pulse, which on average is 58 ps full width at half maximum (FWHM).

Temporal jitter and short term drift between the

532 nm pulses and the dye laser pulses also contribute to the width of the cross-correlation signal. Moreover, such effects determine the time resolution of the pump and probe experiments. They are due largely to cumulative pulse shaping effects in the operation of the synchronously pumped dye laser, and are ultimately caused by intensity fluctuations of the pump laser [31]. This was measured to be $< 2\%$ RMS and the temporal jitter and drift over the course of a single experiment are estimated to be no more than a few picoseconds RMS. However, over a longer period of time, the zero delay point is found to drift by up to 20 ps, most probably due to a drift in the pump laser intensity. For this reason, in order to accurately measure and compare the absolute initiation times for breakdown under different conditions, the cross-correlation between the laser pulses is collected before and after each 6 min experimental run.

Experiments are performed with helium, argon and nitrogen, over a range of pressures from a few Torr to several atmospheres, for probe wavelengths from 565 to 605 nm and over a range of 532 nm pulse energies, corresponding to peak intensities from 10^{13} to 2×10^{14} W cm^{-2}.

In addition to measuring the 'rise-time' of the plasma in each pump and probe experiment, the relaxation time of the plasma was also recorded by collecting the amplitude of dye laser pulses subsequent to the diagnostic pulse. This was achieved by using the boxcar in waveform mode. All data acquisition was automated by controlling the boxcar and translator controller by a personal computer.

3. Experimental conditions and data interpretation

The beam mode of the 532 nm pulses is a close to gaussian, so that the intensity near focus may approximately be expressed in cylindrical coordinates as

$$I(r,z,\theta,t) = \hat{I}\exp(-t'^2/2\sigma_t^2) \times \exp[-2r^2/\omega_0^2(1+a^2z^2)]/(1+a^2z^2) \qquad (1)$$

where $t' = t - z/c$, $\hat{I} = E/(\sigma_t 2^{-1/2} i^{3/2} \omega_0^2)$ is the peak intensity, E is the pulse energy, $\sigma_t = \Delta t/2\sqrt{2\ln 2}$ where $\Delta t = 58$ ps is the FWHM pulsewidth, $\omega_0 = 7.8\ \mu m$ is the beam waist, and $1/a = i\omega_0^2/\lambda = 0.036$ cm is the Rayleigh length.

Because the beam waist is considerably smaller than the Rayleigh length and because intensity falls exponentially ($\exp(-r^2)$) in the radial direction but only quadratically (z^{-2}) in the axial direction, the effective volume of the breakdown region is expected to be a long thin cylindrical shape, as shown in figure 4. By arranging the probe beam to be collinear to the 532 nm beam, the probe pulses sweep through the full length of the breakdown region and are a sensitive indication of the presence of the plasma. Indeed, as the pressure inside the cell is gradually increased, so as to allow the

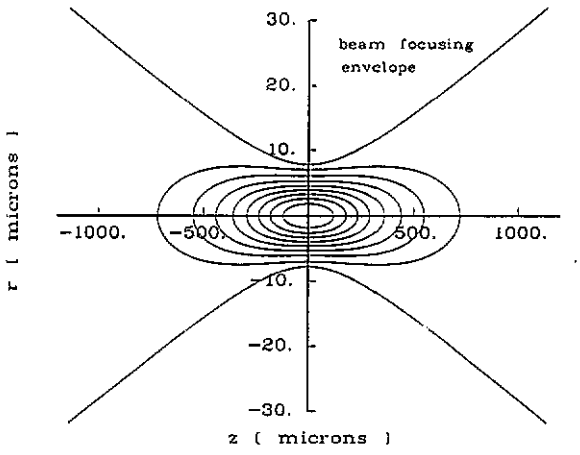

Figure 4. The effective breakdown volume, calculated by equation (1) showing contours of $I/\hat{I}$ from 0.9 to 0.2, and the $1/e^2$ waist of the focused beams. Note that the aspect ratio of $r : z$ has been scaled by 50:1 in this graph, and that the breakdown volume has a long thin cylindrical shape.

formation of a plasma, the probe pulses show some absorption even when the plasma is not strong enough to be visible through the viewing window.

One disadvantage of this high aspect ratio collinear optical configuration is that the overlap volume of the long thin focal regions of the beams is quite dependent on alignment. Consequently, the interaction of the probe pulses with the breakdown region is affected by the pointing stability of the lasers and optical delay line. By averaging the transmission ratio over many laser pulses and scans of the optical delay line, the effects of jitter in the pointing alignments of the lasers are somewhat averaged. Note that the coupling of the probe pulses onto the photodiode is not so sensitive to alignment since the beam passes through the prism and aperture without clipping and is focused tightly into the centre of the photodiode. Note also that the transit time of a light pulse through the long breakdown region is longer than the lengths of the pulses, and for each plasma event the pump and probe pulses simultaneously sweep through the region with a fixed relative time delay.

The maximum pressure used is 7350 Torr, and if at this pressure all atoms were singly ionized to yield an electron density of $n_e = 2.6 \times 10^{20}$ cm^{-3}, the plasma frequency would be $\omega_{pe} = (4\pi n_e e^2/m)^{1/2} = 9.1 \times 10^{14}$ s^{-1}, whereas the frequency of the laser pulses is $\omega > 3.1 \times 10^{15}$ s^{-1}. Thus all experiments are performed in the regime with ω above the critical damping frequency.

Although absorption of the probe pulses by the plasma can be due to molecular dissociation, excitation of metastable states and the many other mechanisms discussed in section 1, in most of our experiments absorption is expected to be due largely to inverse bremsstrahlung, whereby incident radiation induces electronic oscillations, which are damped by electron–ion collisions. If thermal equilibrium does

not prevail, this interaction of the laser pulse with the plasma must be obtained from a detailed computation which takes into account the actual energy distribution function of the free electrons [19, 20]. However, if local thermal equilibrium can be assumed, the complex index of refraction of the plasma will be

$$n = n' + i\kappa = \left(1 - \frac{\omega_{pe}^2}{\omega^2(1 + i\nu_{ei}/\omega)}\right)^{1/2} \qquad (2)$$

where ν_{ei}, the electron–ion collision frequency, depends on the electron density n_e and temperature T_e [2]. From equation (2.37) of reference [2], with n_e in cm^{-3} and T_e in eV, we find

$$\nu_{ei} \sim 2.72 \times 10^{-5} \ln(1.55 \times 10^{10} T_e^{1/2}/n_e^{1/2})\, n_e/T_e^{3/2}. \qquad (3)$$

For the most dense plasmas used in this work, even if the boundary of the plasma were abrupt and the electron–ion collision frequency were taken to be very large, ($\nu_{ei} \sim 6 \times 10^{15}\ s^{-1}$) the reflection coefficient from the boundary, $R = (n-1)(n^*-1)/(n+1)(n^*+1)$, would be less than a few per cent.

On the other hand, the radial gradient of the electron density may cause the developing plasma to act as a weak concave lens which could give rise to refraction of the probe pulses. While refraction clearly occurs for the more dense plasmas, as seen by an increase in the size of the 532 nm beam transmitted by the plasma, for experiments at lower plasma densities, refraction is not expected to significantly effect the energy of the probe pulse which is collected onto the photodiode. Also, for the long, thin focusing geometry used in these experiments, the plasma expansion shock wave is largely in the radial direction so that interaction of the probe pulses with the shock wave is expected to be minimal [32]. Thus the major causes for the attenuation of the probe pulses are expected to be absorption within the bulk of the plasma, and for the more dense plasmas, refraction of the probe beam due to the lens effect of the radial gradient of the plasma density.

If refraction is ignored, the extinction coefficient, κ in equation (2), would cause the probe pulse intensity to decay exponentially with propagation distance with a linear absorption coefficient

$$K = 2\omega\kappa/c. \qquad (4)$$

The net transmission ratio, T, of a plane-wave probe beam, after propagation through a uniform slab of plasma of electron density n_e and effective temperature T_e would then be found from equations (2)–(4) and is shown in figure 5 for a slab thickness of $2/\alpha = 0.072$ cm. For the expected range of n_e and T_e in our experiments, the predicted transmission ratio is comparable to our experimentally observed values presented in section 4 below. Thus by making simplifying approximations about thermal equilibrium and the plasma geometry, and assuming a particular plasma temperature and thickness, it becomes straightforward to transform the experimentally measured probe-pulse transmission ratio to give

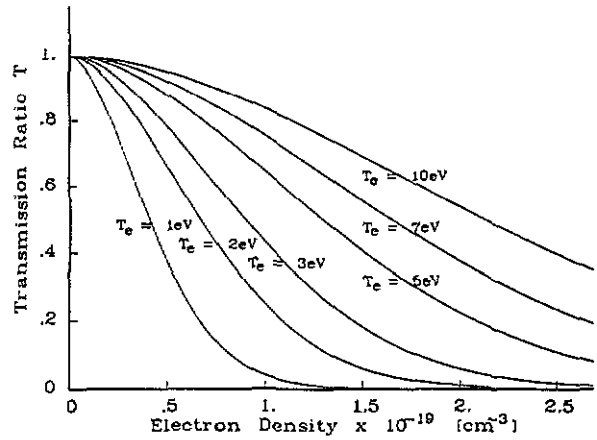

Figure 5. Predicted transmission ratio versus electron density over a range of electron temperatures for a slab of plasma of thickness 0.072 cm (i.e. twice the experimental Rayleigh length). Note that at one atmosphere the electron density is $2.7 \times 10^{19}\ cm^{-3}$ if there is one free electron for each molecule.

the growth in the electron density with time, thereby permitting a comparison of the predictions of existing models [18–21] with the experimental results.

In reality, however, the evolving breakdown plasma does not have a constant temperature or thickness and moreover it is not uniform or in thermal equilibrium, but the electron density and energy distribution evolve as functions of space and time and mechanisms other than inverse bremsstrahlung also contribute to the absorption. A more detailed understanding of laser initiated breakdown in realistic but simple experimental geometries will thus require an extension of the existing numerical models [18–21] to the three-dimensional cylindrically-symmetric geometry described by equation (1). An extended model could also be used to evaluate the absorption and refraction of the probe pulses by the developing plasma, since the probe pulses are collinear and have almost the same gaussian beam parameters as the 532 nm breakdown pulses.

Thus the experimental transmission ratios presented in the following section should serve as valuable points of comparison with the predictions of future computationally-intensive models. In addition, the experimental data exhibit interesting features which confirm that thermal equilibrium should not be assumed for model simulations at low pressures and this is discussed with the results below.

4. Results and discussion

In figure 6 we show the transmission ratio of 590 nm probe pulses due to the breakdown in nitrogen gas at a pressure of 50 Torr for a range of 532 nm pulse energies, as given in the figure. The initiation time of the plasma is seen to occur at earlier times for larger pulse energies. The rate of growth of the plasma as indicated by the rate of change of the transmission ratio is seen to be larger for larger pulse energies. Also, the transmission ratio is

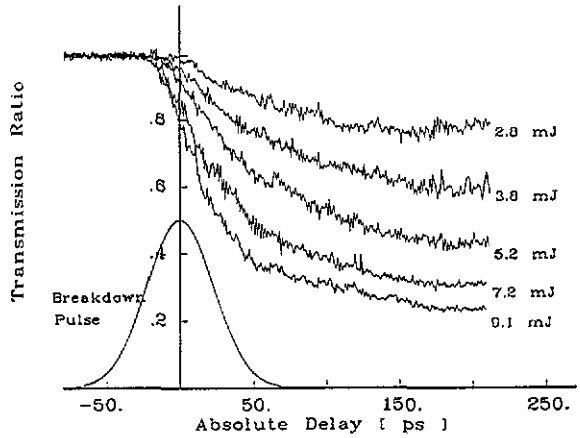

Figure 6. Breakdown in nitrogen, at a pressure of 50 Torr, for varying pulse energies. At the maximum pulse energy of 9.1 mJ, the peak intensity is 1.5×10^{14} W cm^{-2}.

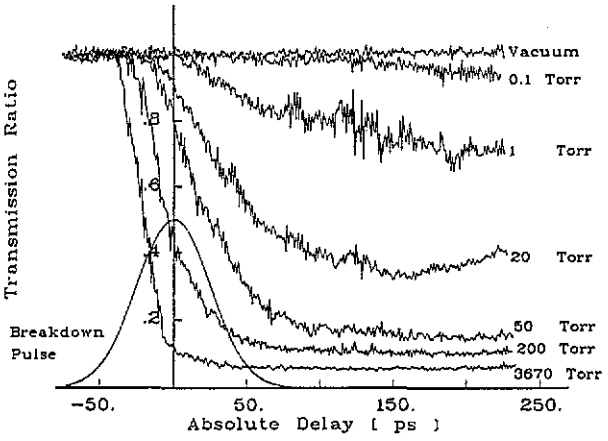

Figure 7. Breakdown in nitrogen, at varying pressures, for a mean pulse energy of 9.5 mJ. This corresponds to a peak intensity of 1.6×10^{14} W cm^{-2}.

seen to continue to fall for times after the breakdown pulse has passed, indicating that the plasma continues to grow due to its internal energy rather than externally supplied energy.

In figure 7 we show the transmission ratio of 590 nm probe pulses due to the breakdown in nitrogen gas for a 532 nm pulse energy of 9.5 mJ over a range of pressures up to 3670 Torr. At the lower pressures the plasma continues to grow after the breakdown pulse has passed. Even for a pressure as low as 0.1 Torr, some decrease in the transmission ratio of the probe pulse is seen hundreds of picoseconds after the breakdown pulse has passed. At this pressure and at a pressure of 1 Torr, the plasma was not visible. That this change in the transmission ratio is due to a phenomena within the nitrogen rather than a nonlinear effect at the cell windows or other optics is demonstrated by the absence of change when the cell is completely evacuated.

The production of the first energetic electrons is expected to be due to multiphoton ionization caused by the breakdown pulse. Above threshold, ionization and ponderomotive acceleration of the electrons can result in highly energetic electrons [33]. For pressures

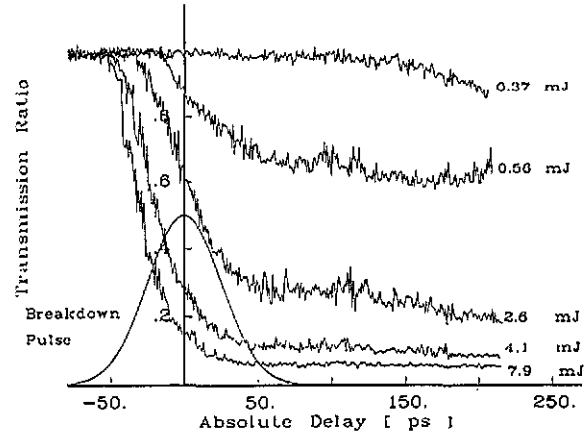

Figure 8. Breakdown in argon, at a pressure of 1570 Torr, for varying pulse energies. At the maximum pulse energy of 7.9 mJ, the peak intensity is 1.3×10^{14} W cm^{-2}.

as low as 0.1 Torr, the electron-ion collision frequency, which largely determines the rate of electron energy loss, and the electron-neutral collision frequency, which determines the rate of cascade growth, are expected to be very slow [19]. Thus it is quite reasonable to expect that a condition of non-equilibrium persists and that this is responsible for the continued growth of the plasma after the breakdown pulse has passed.

In figure 7, as the pressure is increased, the rate of growth of the plasma increases and the initiation time of the plasma moves to earlier times. At a pressure of 3670 Torr, we see a 66% change in transmission ratio over a timescale of only 20 ps, whereas the breakdown pulse has a width of $2\sigma_t = 50$ ps (FWHM= 58 ps), i.e. the breakdown is considerably faster than the 532 nm pulse.

The temporal characteristics of the breakdown in argon appear similar to those in nitrogen, although the pressure or pulse energy required to obtain breakdown is higher. The transmission ratio of 590 nm probe pulses for breakdown in argon at a pressure of 1570 Torr and for a range of 532 nm pulse energies is shown in figure 8. The observation of an earlier breakdown initiation time for higher pulse energy is in agreement with the predictions of the model calculation for the growth of ionization in argon given in [21]. A similar shift to earlier initiation times for higher pressures is seen in figure 9 which shows the probe pulse transmission ratio for breakdown in argon over a range of pressures up to 1500 Torr, for a 532 nm pulse energy of 10.3 mJ.

Breakdown in helium was only found to occur at higher pulse energies and pressures. We were not able to observe the very weak absorption of the probe pulses which occurs after the breakdown pulse has passed and which initiates in the trailing edge of the breakdown pulse, as was observed for nitrogen and argon. Figure 10 shows the transmission ratio versus delay of a 590 nm probe pulse through a helium plasma caused by a 9.5 mJ 532 nm pulse over a range of pressures. At the higher pressures the growth of the plasma is seen to be quite abrupt, consistent with the expectation

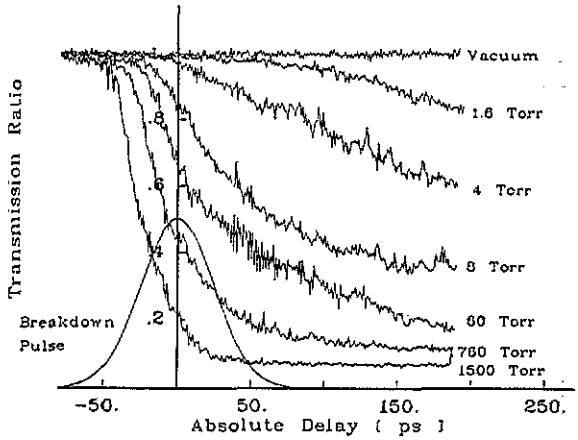

Figure 9. Breakdown in argon, at varying pressures, for a mean pulse energy of 10.3 mJ. This corresponds to a peak intensity of 1.7×10^{14} W cm^{-2}.

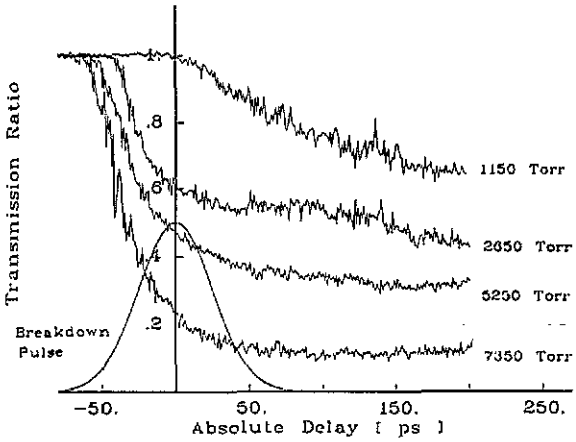

Figure 10. Breakdown in helium, at varying pressures, for a mean pulse energy of 9.5 mJ. This corresponds to a peak intensity of 1.6×10^{14} W cm^{-2}.

that growth proceeds by cascade ionization under these conditions.

Experiments were performed over a range of dye laser probe wavelengths, λ, for a fixed 532 nm pulse energy and gas pressure. These experiments did not detect an appreciable change in the shape of the curves of the transmission ratio versus delay, but, in general, the absorption of the probe pulses was found to be considerably greater at longer wavelengths. For inverse bremsstrahlung, the absorption is expected to increase at longer wavelengths approximately as λ^2. This does not fully account for the observed wavelength dependence, and a stronger wavelength dependence has been attributed to the increasing importance of multiphoton ionization and ionization from excited states for visible wavelengths [19].

Figure 11 shows the case of breakdown in helium probed at four different wavelengths. Here we find that the probe pulse absorption increases steadily as the wavelength is increased, except for a sharp peak in absorption at 586 ± 2 nm, which corresponds to the 587.8 nm $2p\,^3P^0 \rightarrow 3d\,^3D$ transition in the spectrum of neutral helium. At 586 nm the absorption is about

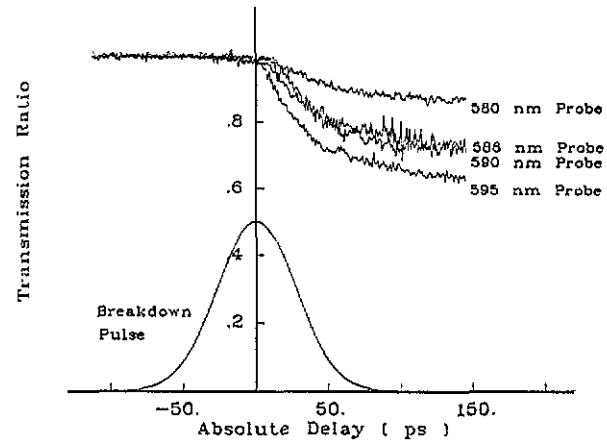

Figure 11. Breakdown in helium, at a pressure of 1570 Torr, for a mean 532 nm pulse energy of 7.1 mJ, corresponding to a peak intensity of 1.2×10^{14} W cm^{-2}, as seen by picosecond probe pulses at four different wavelengths. There is a steady increase in the absorption of probe pulses as the wavelength is increased, except at 586 ± 2 nm, for which an enhanced absorption is observed.

the same as that at 590 nm, whereas at 585 nm the absorption is found to be about midway between that at 580 nm and that at 590 nm.

In addition to measuring the transmission ratios versus delay, at each condition of pressure, breakdown pulse energy and different gas type, the waveform from the dye laser pulses is collected up to 200 ns following breakdown. From the change in the absorption of the dye laser probe pulses over this period, we can monitor the relaxation of the plasma. Figure 12 shows the waveform collected from a helium plasma at moderate pressure showing an incomplete recovery of the plasma with a half-lifetime of about 50 ns. While some of the pulse-to-pulse fluctuations of the transmitted dye laser pulses shown in this waveform are due to radio-frequency pick-up of noise from the regenerative amplifier flashlamp discharge, most of the fluctuations are found to be critically dependent on the collinear alignment of the pump and probe laser beams. If this alignment is deliberately misadjusted, clear oscillations in the transmission of the dye laser probe pulses can be seen. This is possibly due to refractive loss of the probe beam from the shock wave which develops after breakdown. Such effects would make quantitative measurements of the relaxation of the plasma absorption by this method very difficult.

Nevertheless, qualitative features of the plasma relaxation can be discerned and appear to be consistent with a more comprehensive published account of the relaxation of hydrogen plasmas [34]. For all three gases, the relaxation time is found to be approximately linearly dependent on pressure and may be as short as 10 ns or longer than 100 ns. In the case of helium plasmas, when the probe pulse wavelength is changed to 586 ± 2 nm, corresponding to the $2p\,^3P^0 \rightarrow 3d\,^3D$ transition, as shown in figure 13, the absorption of the probe pulses continues to increase for about 10 ns and while

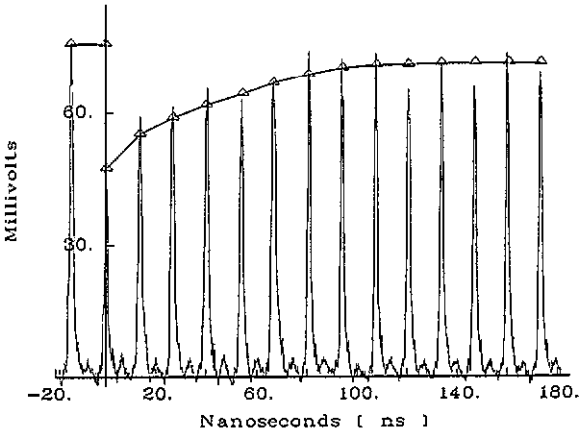

Figure 12. The waveform collected from breakdown in helium, at a pressure of 1570 Torr, for a pulse energy of 7.1 mJ, corresponding to a peak intensity of 1.2×10^{14} W cm^{-2}, using picosecond probe pulses at a wavelength of 590 nm. The plasma absorption is seen to give incomplete relaxation with a half-life of $\sim$ 50 ns.

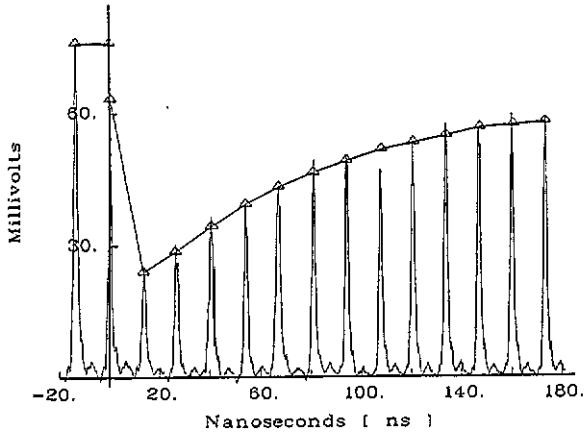

Figure 13. The waveform collected from breakdown in helium, at the same conditions as in figure 11, but using picosecond probe pulses at a wavelength of 586 $\pm$ 2 nm. The plasma absorption is seen to grow for about 10 ns after breakdown and then give incomplete relaxation with about the same half-life of $\sim$ 50 ns.

the time constant for the relaxation of the probe pulse absorption is about the same, the residual absorption after 200 ns is greater. This residual absorption is possibly due to the presence of metastable states which relax to the $2p^3P^0$ state.

5. Conclusions

We have used a collinear pump and probe technique to measure the temporal response of laser breakdown plasmas in nitrogen, argon and helium, with a resolution of a few picoseconds. The high f-number focusing geometry used, results in a long thin breakdown volume which gives high sensitivity to the absorption of the probe pulses by the plasma but which has the disadvantage that the response of the probe pulses is dependent on exact collinear beam alignment.

Several features in the temporal response of the breakdown and plasma growth have been noted. For example, at low pressures in argon and nitrogen, growth of the plasma continues after the breakdown pulse has passed, while at high pressures, in all gases, the breakdown is seen to be quite abrupt compared with the duration of the breakdown pulse. The relaxation time of the plasma absorption was also measured and this is found to be pressure dependent with a half-life of up to 100 ns for a pressure of several atmospheres.

Acknowledgments

This project was supported by AFOSR grant number AFOSR-86-0317. We thank Q Zhang and A Sedghinasab for assistance with initial experiments and B Hill, J Hornkohl, F Schwartz and N Wright for technical assistance.

References

[1] Weyl G M 1989 *Laser-Induced Plasmas and Applications* ed L J Radziemski and D P Cremers (New York: Marcel Dekker) pp 1–67
[2] Hora H 1981 *Physics of Laser Driven Plasmas* (New York: Wiley)
[3] Zeldovic Y B and Raizer Y P 1965 *Sov. Phys. JETP* **20** 772
[4] Chan C H, Moody C D and McKnight W B 1973 *J. Appl. Phys.* **44** 1179
[5] Brown R T and Smith D C 1973 *Appl. Phys. Lett.* **22** 245
[6] Agostini P, Barjot G, Mainfray G, Manus C and Thebault J 1970 *IEEE J. Quant. Elect.* **6** 782
[7] Baravian G, Godart J and Sultan G 1982 *Phys. Rev.* A **25** 1483
[8] Keldysh L V 1965 *Sov. Phys. JETP* **20** 1307
[9] Boreham B W and Luther-Davies B 1979 *J. Appl. Phys.* **50** 2533
[10] Fittinghoff D N, Bolton P R, Chang B, Van Woerkom L D and White W E 1991 *SPIE Tech. Proc.* **1413** 81
[11] Augst S, Meyerhofer D D, Strickland D and Chin S L 1991 *J. Opt. Soc. Am.* B **8** 858
[12] Gamal Y E and Harith M A 1983 *J. Phys. D: Appl. Phys.* **16** 1901
[13] L'Huillier A, Mainfray G and Johnson P M 1984 *Chem. Phys. Lett.* **103** 447
[14] Gamal Y E and Abdel-Moneim N M 1987 *J. Phys. D: Appl. Phys.* **20** 757
[15] Minck R W 1964 *J. App. Phys.* **35** 252
[16] Krasyuk I K, Pashinin P P and Prokhorov A M 1970 *Sov. Phys. JETP* **31** 860
[17] Dewhurst R J 1978 *J. Phys. D: App. Phys.* **11** 191
[18] Rosen D I and Weyl G 1987 *J. Phys D: Appl. Phys.* **20** 1264
[19] Weyl G M and Rosen D 1985 *Phys. Rev.* A **31** 2300
[20] Kroll N and Watson K M 1972 *Phys. Rev.* A **5** 1883
[21] Phelps A V 1966 *Physics of Quantum Electronics* ed P Kelley *et al* (New York: McGraw-Hill) pp 538–547
[22] Stricker J and Parker J G 1982 *J. Appl. Phys.* **53** 851
[23] Armstrong R A, Lucht R A and Rawlins W T 1983 *Appl. Opt.* **22** 1573
[24] Ireland C L M, Yi A, Aaron J M and Grey Morgan C, 1974 *Appl. Phys. Lett.* **24** 175
[25] Alcock A J, DeMichelis C, Hamal K and Tozer B A 1968 *IEEE J. Quant. Elect.* **4** 593
[26] Yablonovitch E 1974 *Phys. Rev.* A **10** 1888

[27] Rolland C and Corkum P B 1986 *J. Opt. Soc. Am.* B 3 1625
[28] Dhareswhwar L J, Naik P A and Bhawalkar D D 1991 *Rev. Sci. Instrum.* **62** 369
[29] Kapteyn H C, Murnane M M, Szoke A and Falcone R W 1991 *Opt. Lett.* **16** 490
[30] Lencioni D E 1973 *Appl. Phys. Lett.* **23** 12; 1974 *Appl. Phys. Lett.* **25** 15
[31] Davis L M, Harvey J D and Peart J M 1984 *Opt. Commun.* **50** 49
[32] Tomlinson R G 1971 *Appl. Phys. Lett.* **18** 149
[33] Freeman R R, Bucksbaum P H, Milberg H, Darack S, Schumacher D and Geusic M E 1987 *Phys. Rev. Lett.* **59** 1092
[34] Litvak M M and Edwards D F 1966 *J. Appl. Phys.* **37** 4462